IEEE Access
Multidisciplinary | Rapid Review | Open Access Journal

Received September 9, 2021, accepted October 10, 2021, date of publication October 13, 2021, date of current version October 19, 2021.

Digital Object Identifier 10.1109/ACCESS.2021.3119748

Technology Assessment of Aperture Coupled Slot Antenna Array in Groove Gapwaveguide for 5G Millimeter Wave Applications

IVAN ZHOU, LLUÍS JOFRE, (Life Fellow, IEEE), AND JORDI ROMEU, (Fellow, IEEE)
Department of Signal Theory, Universitat Politècnica de Catalunya (UPC), 08034 Barcelona, Spain

Corresponding author: Ivan Zhou (ivan.zhou@upc.edu)

This work was supported in part by the Agencia Estatal Investigación under Grant PID2019-107885GB-C31/AEI/10.13039; and in part by the Catalan Research Group under Grant 2017SGR219, Grant MDM2016-O6OO, and Grant DI2020-043.

ABSTRACT A compact triple-layer series fed slot unit array using Groove Gap Waveguide (GGW) technology for 5G millimeter-wave applications is presented in this paper. The design employed a two-step coupling mechanism for the radiating slots. The aperture coupling design when combined with the groove gapWaveguide (GGW) technology allows achieving three different goals: First, a reduction of the array size in the transversal direction, so more unit arrays can be added without grating lobes. Secondly, low insertion losses with high radiation efficiency. And third, a reduction of the manufacturing complexity with good stability against fabrication tolerances of up to 0.1 mm, making the design feasible to be massively deployed. The antenna was fabricated and measured showing good agreement with the numerical simulation results, the antenna provides a peak realized gain of 12.15dB at the central frequency of operation and a fractional bandwidth (FBW) of 9%.

INDEX TERMS Compact antenna, series fed slotted array, 5G millimeter wave antennas, robust antenna.

I. INTRODUCTION

The increasing demand for high data speed, such as 8K video streaming and virtual augmented realities is expected to fold-1000 the data traffic in the upcoming decade [1]. Exploring new less-congested spectrum bands of high frequencies such as the millimeter-wave (mmWave) bands (30 - 300 GHz) is a promising solution to increase network capacity. However, new architectures with densification of small-cell technologies are required to mitigate propagation losses, reduce interference and increasing coverage [2]. Such densification requires the extensive deployment of dense wireless networks such as backhaul, for aggregating and sending data traffic from the radio access to the (wired) backbone segment or the cost-effective 5G smart repeaters to ensure a complete wireless coverage in difficult urban spots, among many other requirements. In this regard, high-gain antennas robust to manufacturing tolerances are required for the massive distribution of wireless network nodes. 5G mmWave band comprises the FR2 band, with frequencies ranging from 24.25GHz to 48.2 GHz where smart repeaters and many backhaul applications work on. However, the FR2 band for the latter one is not sufficient to deliver today's capacity peaks [3], offloading to E-band (71-76GHz and 81-86GHz) spectrum is taking place.

In addition, a minimum antenna gain of 43 dB at E-Band is imposed by the FCC to 5G Backhaul cells, which requires a large antenna size such as 1-foot parabolic antennas, compared to 5G smart repeaters only 22 dB is required. Companies such as Ericsson and Nokia, alongside Avit and Comsearch pushed to decrease the antenna gain requirement to 38 dB in order to support smaller antennas, so integration in equipment at the street level such as light poles can be easier [4]. There is a clear trend to reduce the antenna size, so a more compact solutions can be adopted. It is obvious that gain requirements fix the minimum antenna dimension but a technology with higher efficiency and smaller thickness requirements will be preferred. More integrated solutions have been proposed such as horn arrays [5], transmit arrays [6], and lens antennas [7] but the size is still too bulky to be easily fitted on urban equipment.

In this context, compact low-thickness, high-efficiency, high-gain antennas with good fabrication tolerance stability are required for 5G mmWave network deployments. When

The associate editor coordinating the review of this manuscript and approving it for publication was Mohammad Tariqul Islam.

referring to very compact solutions traditional arrays are an attractive solution and can be mainly classified into corporate feeding networks and series fed arrays. The first is more commonly used for fixed point-to-point communications while with the latter technique, a phased array solution can be implemented making it more preferable.

Conventional series-fed arrays in a microstrip line can be found in [8] and [9]. However, the losses with dielectric and its uncertainties on the actual value of permittivity make it difficult to correlate the measured results with the simulations at these high frequencies. Waveguides can solve these problems as the dielectric is avoided by using four sealed walls to guide the electromagnetic wave through the air medium. Similar arrays in rectangular waveguide (RW) can be found in the literature by implementing slots, and they are mainly classified into two categories, vertical rectangular waveguide (V-RW) or narrow wall slots [10] and horizontal rectangular waveguide (H-RW) or broad wall slots [11]. Regarding V-RW, they offer more compactness in the antenna plane so beam steering capabilities using $\lambda/2$ separated unit arrays can be achieved without many dimensional restrictions as well as a considerable reduction in sidelobe level (SLL). However, the slots must be excited using a tilt angle as currents are in counter phase every $\lambda_g/2$ [12], [13], which is highly undesirable as cross polarization (CPol) appears. Many studies have been conducted in order to make these elements radiate in phase while maintaining low levels of CPol by using parasitic elements inside the waveguide to modify the current distribution [14]; however, a very demanding manufacturing precision is required and they are bandwidth limited. In addition, fast prototyping of waveguides needs to be manufactured on separate pieces, requiring perfect sealing when unifying them in order to avoid leakage [15].

In this context, gapWaveguide (GW) has attracted attention during the last decade, and the invention by S. Kildal offers a contactless full metal two parallel plates guiding structure solution by using an artifitial magnetic conductor (AMC) at both sides of the transmission line, so all the electromagnetic energy is confined by the parallel plates and the AMC [16]. The AMC can be achieved by rows of periodic nails, although other conformations can be adopted such as mushrooms type [17], with the only condition that the space between the AMC and the parallel plate is smaller than $\lambda_g/4$. Clearly, in this configuration, there is no need for an electrical connection between the top and bottom conductive planes of the waveguide, leading to a low loss and relatively easy manufacturing process.

In order to benefit from the advantages of the GW technology, different designs have been reported in the literature, which can be classified into two main groups, ridge gapWaveguide (RGW) [18] which is the most popular design owing to its analogy to the microstrip line but in an inverted form and GGW [19] with a working principle similar to that of RW. There are two subgroups of GGW technology: named horizontal groove gapWaveguide (H-GGW) and vertical groove gapWaveguide (V-GGW). Some designs have been made on H-GGW [20] but the size is too long in the transversal direction of the array similar to H-RW. Only a few works have been published to solve the problems of slot excitation using V-GGW, in [21] parasitic dipole elements are used in the upper layer by means of an extra layer of substrate; however, it only shows 2% FBW.

TABLE 1. Comparison with other similar works. The minimum separation parameter from the fifth column is the minimum inter-array separation achievable of the design, η is the measured efficiency.

Ref.	Tech.	CPol	FBW (%)	Min. separation (λ)	Thickness (λ)	η
Conventional Integrated Solutions						
[5]	Horn	No	29.5	NA	4	NA
[6]	TA	No	15.4	NA	11	48
[7]	Lens	No	NA	NA	27	NA
Series fed Solutions						
[9]	Micros.	No	7	0.55	0.03	39
[11]	H-RW	No	6.2	1.3	0.7	90.2
[12]	V-RW	Yes	2.1	0.5	0.7	NA
[13]	V-RW	Yes	9	0.5	0.7	80
[14]	V-RW	No	6.4	0.29	0.61	NA
[20]	H-GGW	No	2.8	1.32	0.33	93
[21]	V-GGW	No	2	0.57	0.75	NA
[22]	RGW	No	14.4	0.65	0.7	NA
[23]	RGW	No	3.8	0.49	0.165	NA
This work	V-GGW	No	9	0.57	1.91	92.2

In comparison to the antennas presented in the literature (see Table 1), we propose a new method for exciting narrow wall slots from V-GGW without added manufacturing complexity and a good fabrication tolerance stability of up to 0.1 mm (corresponding to the tolerances of a conventional manufacturing technique). The antenna consists of a triple-layer structure with a novel aperture coupling mechanism offering a linearly polarized, high efficiency (92.2%) with a high measured FBW (9%) while being compact in the transversal direction, so the gain can be simply increased by just adding more unit arrays along the transversal direction of the array without having large SLL.

The paper is organized as follows, in the next section II the antenna structure and working principle are described, section III shows a study of the tolerance in different GW technologies and a comparison with a conventional design of series fed array in RGW is made at simulation level, in section IV the results of the measured prototype and simulated ones are correlated and concluded in section VI. In section V the limitations of the work done in this study are also introduced.

II. ANTENNA DESIGN

The challenge in the development of new highly integrable antennas for urban 5G mmWave wireless nodes raises the

demand for new compact solutions with low fabrication precision requirements, high efficiency, and high gain with beam-pointing requirements in some scenarios. Series fed slots in V-GGW technology were chosen as a good candidate because of three main reasons. First, with only one excitation port, all the elements radiate in phase, reducing the complexity of the feeding network when compared to corporate feeding. Second, the antenna is compact in the transversal direction of the array, so gain can be increased by simply adding 0.5λ spaced arrays in that direction without losing beam steering capabilities. Finally, it offers an easy assembly process.

A. SLOT EXCITATION PROBLEM

The slot elements from a series fed design in the narrow wall of vertically oriented waveguide-related technologies cannot be directly excited as stated in the introduction.

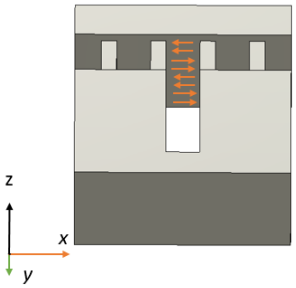

(a) Inclined V-GGW structure

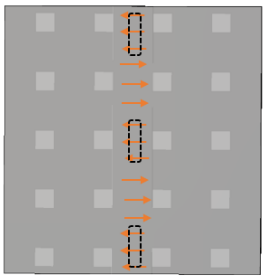

(b) Direct solution

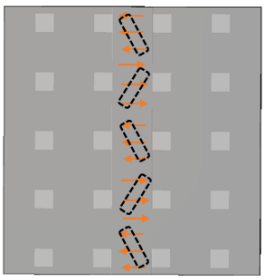

(c) Conventional solution

FIGURE 1. (a) V-GGW transmission line structure showing the electric currents over the surface of the top wall in orange, they are in phase every λ_g (b) Solution to excite λ_g spaced longitudinal slots in V-GGW (c) Solution to excite $0.5\lambda_g$ spaced slots in V-GGW.

The currents from the top wall of the V-GGW are in counter phase every $0.5\lambda_g$ and oriented towards the transversal direction of the transmission line (see Fig. 1). Longitudinal slots can be implemented (see Fig. 1) (a) with a spacing of λ_g in order to radiate in phase; however, this will result in large grating lobes. A conventional method to keep the elements radiating every $0.5\lambda_g$ as shown in Fig. 1 (b) is performed by using tilted slots, however this will result in high levels of CPol. Many studies have been carried out using intrusion elements or an extra layer of substrate-based radiating elements as stated in the introduction an antenna with no grating lobes and low CPol level can be achieved at the same time. However, they are either bandwidth-limited or require a high manufacturing precision. An isometric and top view of the proposed unit array antenna for this study with $0.5\lambda_g$ radiating slots in V-GGW technology can be seen in Figs. 2 and 3 respectively.

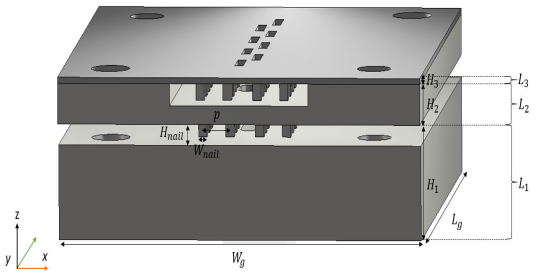

FIGURE 2. Isometric view. Bottom layer L_1, middle layer L_2 and top layer L_3.

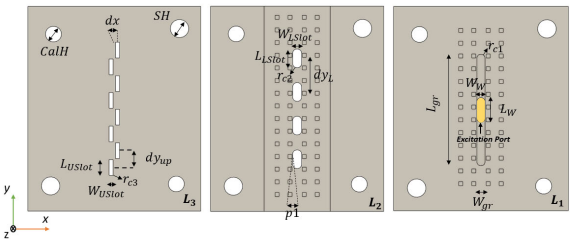

FIGURE 3. Top view of the three different layers. In yellow it is highlighted the input excitation port to the antenna prototype and r_{c1}, r_{c2}, r_{c3} represent the radius of curvature of the flagged edges.

B. PROPOSED ANTENNA

The V-GGW antenna is mainly composed of three layers: the feeding layer (bottom) L_1, coupling layer (middle) L_2 and radiating layer (top) L_3, whose dimensions are listed in Tab. 5. In the bottom layer L_1 there is a direct transition from WR-10 to GGW which consists of a slot ($W_W \times L_W \times H_W$) with corners of r_{c1} radius of curvature. An H-Plane power divider [24] is used to make a central feeding possible in order to achieve symmetrical fields at the radiating elements. The power divider is matched through a stepped transition inserted just below the middle layer L_2 with dimensions ($W_{t1} \times L_{t1} \times H_{t1}$) and ($W_{t2} \times L_{t2} \times H_{t2}$) as shown in Fig. 4.

The groove line ($W_{gr} \times L_{gr} \times H_{gr}$) has rounded ends with r_{c1} radius of curvature. All the energy from the guiding line propagates through four slots ($W_{Lslot} \times L_{Lslot}$) from the middle layer L_2 with corners of tye r_{c2} radius of curvature. These slots are approximately spaced λ_g from each other so they radiate in phase and each one of them, excites two of the eight $\lambda_g/2$ spaced slots of ($W_{USlot} \times L_{USlot}$) from the top layer L_3 with a curvature radius of r_{c3}. In this manner, all the slots radiate in phase with no grating lobes or high CPol level problems.

A symmetrical optimized distribution was considered for the radiating slots, where the intensity of the coupled fields

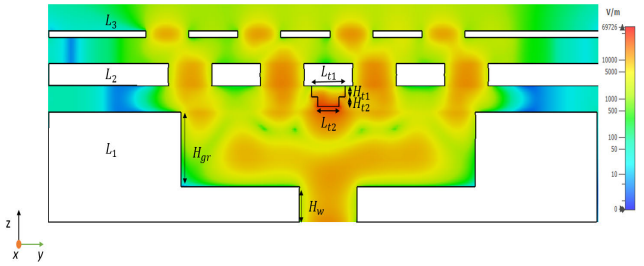

FIGURE 4. Electric Field distribution in linear scale in the x = dx plane cut.

was adjusted by L_{gr} and the offset of the radiating slots dx in order to achieve the lowest SLL while maintaining a high FBW. Lower SLL distributions such as Chebyshev and Taylor can be implemented using a non-uniform offset dx of radiating slots from the top layer L_3 to adjust the coupled energy.

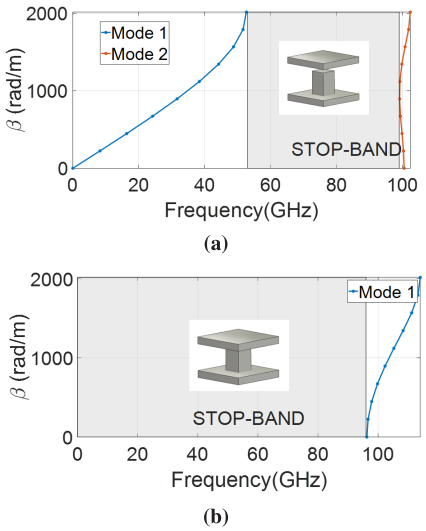

FIGURE 5. (a) With air gap = 0.25λ and (b) direct contact, being the height of the nails of 0.95 mm, width of 0.5 mm and periodicity of 1.6 mm.

The central elements from layers L_1 and L_2 are surrounded by a bed of nails with direct contact with the upper layer and a small spacing p1 with respect to the groove line. It acts as an AMC that prevents leakage through the sides of the transmission line. The dimensions of the bed of nails must be designed to ensure a good AMC performance at the frequencies of interest. A fast calculation of the modes of propagation can be performed by defining the unit cell of the bed of nails via the eigenmode solver from the CST simulator. In Fig. 5 the stopband of the AMC structure ranges from 60 GHz to 100 GHz if an air gap of 0.25λ is left between the upper layer and the nails, and 0-100GHz if they are in direct contact. If the nails are in contact with the upper layer, one single row of nails would be sufficient as will be demonstrated in the experimental section IV, resulting in a more compact unit array (0.57λ of minimum width x 1.91λ height). Two calibrated metallic screws ($CalH$) were used to prevent misalignment between the layers and two metallic screws (SH) to fix the separation between the layers.

III. TOLERANCE ANALYSIS

The massive deployment of antennas requires an important analysis of the manufacturing tolerances. In order to ensure a good radiation performance for N antennas with fabrication tolerances of up to 0.1mm (which is a standard manufacturing tolerance for many industrial technologies) at high frequencies like E-Band is one of the main challenges that this paper has focused on. Gap waveguide technology was selected mainly because of its low loss and easy assembly properties.

A. DESIGN

A first test consisted of a comparison between the impedance stability of the three types of GW, the H-GGW, V-GGW and RGW when introducing dimensional errors of ±0.1mm in order to check the impedance stability of each technology.

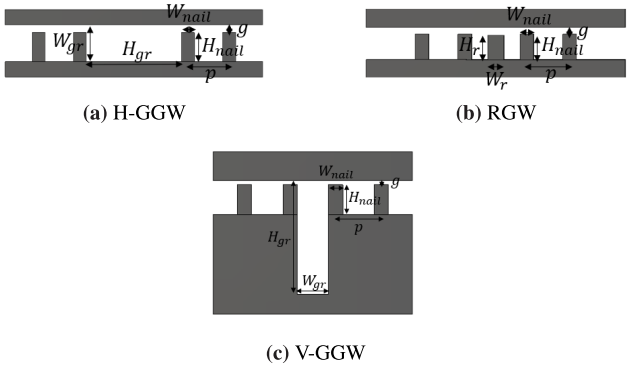

FIGURE 6. Front view of the three main structures in GW technology that are used to analyze the characteristic impedance stability. The AMC structure dimensions are the same for (a), (b) and (c) with a constant air gap g of 0.25 mm between the nail and the top metallic layer.

TABLE 2. Tolerance analysis of the characteristic impedance for each GW technology.

H-GGW			
Parameter	Dimension (mm)	Impedance Zo (Ω)	Relative error (%)
W_{gr}	3.7 ± 0.1	150 ± 1	0.7
H_{gr}	1.05 ± 0.1	150 ± 12	8
H_{nail}	0.95 ± 0.1	150 ± 0.5	0.3
W_{nail}	0.5 ± 0.1	150 ± 0.35	0.3
p	1.6 ± 0.1	150 ± 0.2	0.1
V-GGW			
W_{gr}	1.1 ± 0.1	450 ± 2	0.4
H_{gr}	3.96 ± 0.1	450 ± 34	7.5
H_{nail}	0.95 ± 0.1	450 ± 2.5	0.5
W_{nail}	0.5 ± 0.1	450 ± 1.5	0.3
p	1.6 ± 0.1	450 ± 1.75	0.4
RGW			
W_r	0.6 ± 0.1	100 ± 6	6
H_r	0.9 ± 0.1	100 ± 27.5	27.5
H_{nail}	0.95 ± 0.1	100 ± 0.3	0.3
W_{nail}	0.5 ± 0.1	100 ± 0.25	0.25
p	1.6 ± 0.1	100 ± 0.23	0.23

As we can see in Tab. 2, H-GGW and V-GGW show similar impedance stability where the only critical dimension is the length of the narrow wall, introducing approximately 7.5 - 8 % of relative errors. For the case of RGW, up to 27.5% of the relative error was reached owing to the height of the ridge Hr, making RGW-related designs much more critical to fabrication tolerances. To compare the stability of the radiation pattern and input reflection coefficient with the design of this study, a conventional series fed array in RGW was simulated, as shown in Fig 7.

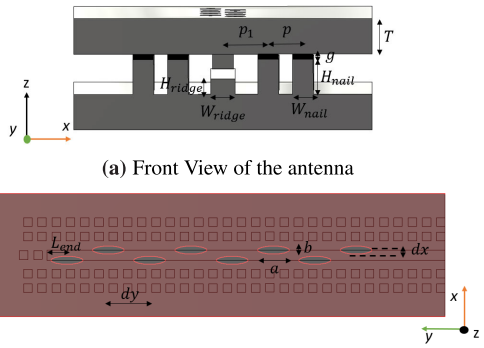

(a) Front View of the antenna

(b) Top View of the antenna

FIGURE 7. Series fed slot array in RGW design.

TABLE 3. Nominal dimensions of the antenna in RGW in mm. Parameters marked with at least one * are used for the tolerance analysis.

Param.	a**	b*	dx*	dy*	Wridge**	Hridge**	Lend*
Dim. (mm)	2.25	0.6	0.5	2.8	0.7	0.7	1.15
Param.	p*	p1*	g**	Wnail*	Hnail*	T*	-
Dim. (mm)	1	1.27	0.1	0.58	1	1.13	-

The antenna also has eight series fed slots with a spacing of approximately $0.5\lambda_g$. Note that only a single layer of radiating slots is needed to directly excite the elements in phase. L_{end} is approximately 0.25λ so all the remaining power is reflected back and a standing wave is created over the array axis. A uniform distribution of the delivered power was used with elliptical slots for bandwidth improvement. All the dimensions of each parameter are summarized at Tab. 3, for a complete description of a similar antenna, see [23].

B. ITERATION OF ERRORS

There are 13 dimensional parameters for the case of RGW design and 31 dimensional parameters for the case of V-GGW, assuming a uniform error distribution with only three discrete values of -0.1, 0 and $+0.1$ mm, see Tab. 4, for every single parameter this would result in a total amount of 1.59 million and over trillions of combined errors respectively, which is obviously not feasible to simulate.

A first analysis of the critical dimensions was carried out to reduce this space of combinations. Errors of $\pm$ 0.1 mm were applied to each parameter separately for the RGW and V-GGW, resulting in 26 and 54 input reflection coefficients,

TABLE 4. Linear sweep used for each dimensional parameter. Each point represents the value that one parameter can get in the whole combined sweep.

Sweep	1	2	3
Value (mm)	Nominal -0.1	Nominal	Nominal+0.1

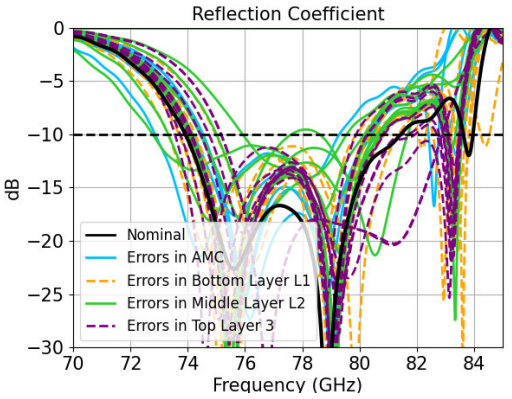

(a)Design in V-GGW.

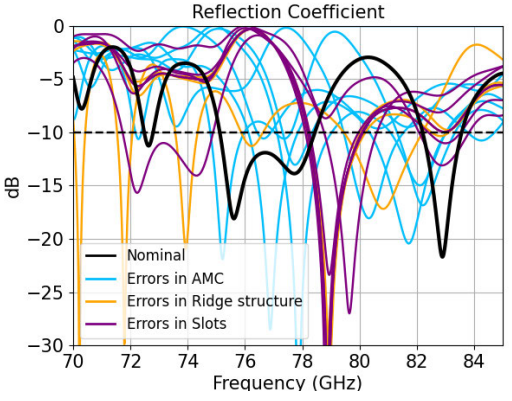

(b) Design in RGW.

FIGURE 8. Simulated input reflection coefficients by adding independently +0.1 mm and −0.1 mm of errors to each dimensional parameter while keeping the rest ones in nominal dimension.

the parameters used in this first study are marked with at least one * in Tab. 3 and Tab. 5 respectively. Some parameters were not included in the tolerance analysis such as the curvature radius (r_{c1}, r_{c2}, r_{c3}) because it is related to the shape rather than dimensional error and, the height of the feeding port (H_W) because it does not affect the impedance of the structure. Parameters from the Tabs. 3 and 5 marked with a double * are the most critical ones in terms of reflection coefficients seen at Fig. 8 (a) and (b) respectively, resulting in a penalty of greater than 15% of FBW reduction if taking into account that the only valid bands for both designs are those marked by the input reflection coefficient when using nominal dimensions. For V-GGW the critical parameters are the length of the slots from each layer L_{Lslot} and L_{USlot}, W_{nail} and $p1$. For the case of RGW the results are much worse (>50% of the FBW penalty) with any parameter. Only these

parameters are selected for the final study using combined errors and are plotted in Figs. 9 and 10.

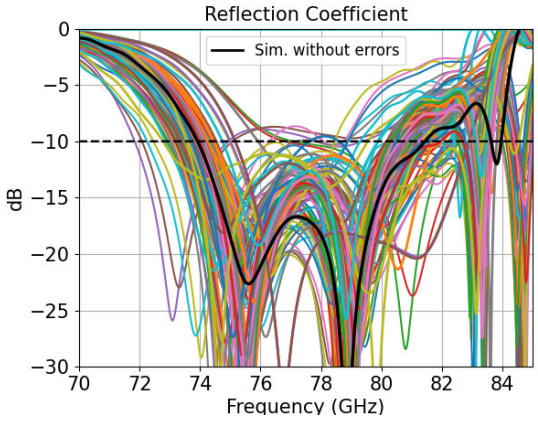

(a)Design in V-GGW. Total amount of 243 combined errors.

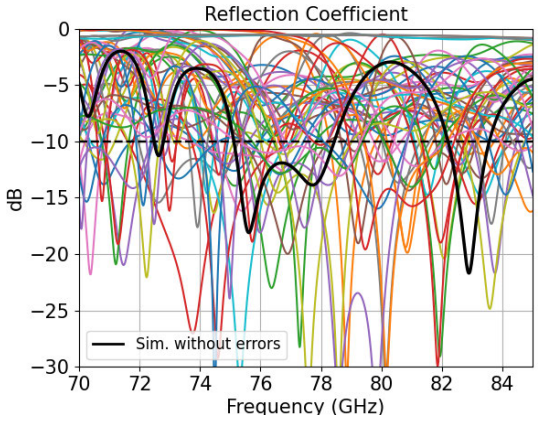

(b) Design in RGW. Total amount of 81 combined errors

FIGURE 9. Input reflection coefficients for the main combination of errors in color, the black trace corresponds to the simulated antenna with nominal dimensions.

For the case of the input reflection coefficients in this V-GGW design, 89% of the combined errors guarantee a frequency range from 74.25GHz to 80GHz, resulting in a 7.5% secured FBW. Clearly, V-GGW shows much better tolerance stability than RGW, as predicted previously in the Design subsection.

Only pattern stability for the design in V-GGW is represented in Fig. 10 because the results are well-matched, showing good pointing stability as well as realized gain. An increase of up to 7.5dB in SLL was due to the errors related to the slot spacing dY_{up} from the top layer L_3. Of course, if considering misalignment errors between each layer, we will have a worse response in terms of SLL although it has almost no impact on the input reflection coefficients.

IV. EXPERIMENTAL RESULTS

The antenna was manufactured using two different methods. $L1$ and $L2$ were fabricated using a standard CNC milling machine from the UPC facilities.

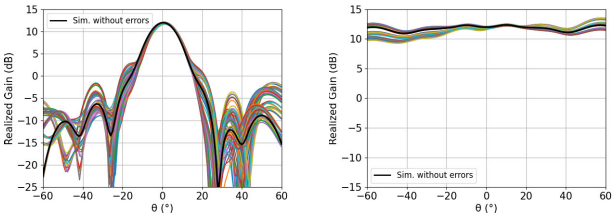

(a) V-GGW H-plane (b) V-GGW E-plane

FIGURE 10. V-GGW design radiation pattern cuts for the main combination of errors in color, - corresponds to the simulated antenna with nominal dimensions. The tolerance of the pattern for the design in RGW was not included as the input reflection coefficients are very mismatched.

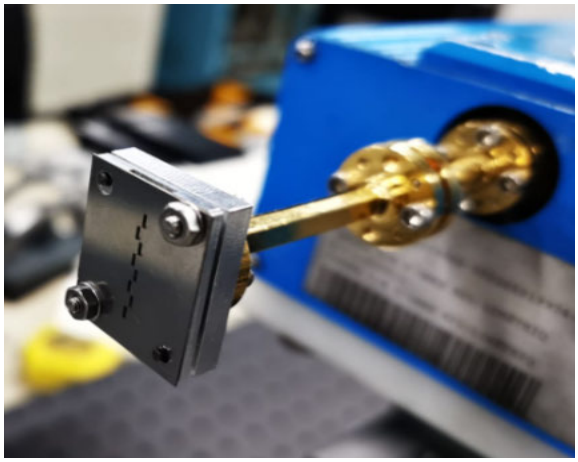

FIGURE 11. Manufactured antenna at the head of the PNA N5222A network analyzer.

TABLE 5. Summary of the main antenna dimensions and the deviations in the fabricated one in mm. The errors for the case of the slots and nails are the maximum errors. Parameters marked with at least one * are used for the tolerance analysis from section III.

Param.	Nom. (mm)	Error (mm)	Param.	Nom. (mm)	Error (mm)
Layer 1			**Layer 2**		
H_{gr}*	2.7	0.02	L_{Lslot}**	2.35	0.07
L_{gr}*	13.95	0.08	W_{Lslot}*	1.1	0.11
W_{gr}*	1	0	dY_L*	4.25	0.05
L_W*	3.1	0.05	r_{c2}	0.5	-
W_W*	1	0.12	H_{t1}*	0.4	0.09
H_W	1.35	-	L_{t1}*	1.55	-0.15
r_{c1}	0.5	-	H_{t2}*	0.35	0.12
H_1*	5	0.03	L_{t2}*	1	-0.17
Layer 3			W_{t1}*	1.1	0
			W_{t2}*	1.1	0
			H_2*	1.75	-0.04
L_{USlot}**	2	0.03	**AMC**		
W_{USlot}*	0.5	-0.01			
dY_{up}**	2.25	0.01	p *	0.88	0.03
$DispX3$*	0	0.15	W_{nail}**	0.5	0.07
$DispY3$*	0	-0.10	H_{nail}*	0.95	0.01
dx*	0.4	0	p1**	0.1	0.05
r_{c3}	0.025	-	H_3*	0.25	0

$L3$ was fabricated externally using laser cutting technology as the width of the slots was too thin to be performed at our facilities. Fabricated dimensional errors are listed in

Tab. 5, which were measured using the Nikon Measurescope MM-11 with a precision of 10um. Pictures showing the main fabricated parts of the structure are shown in Fig. 12.

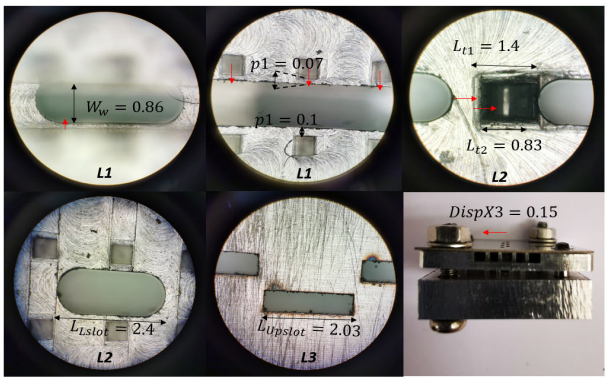

FIGURE 12. Manufactured antenna seen by the microscope, showing the main parts of the structure.

The most deviated errors were caused by the displacement of the $L3$ layer ($DispX3$ and $DispY3$), the connection of the WR10 (W_W) to the waveguide structure, the width of the slots W_{Lslot} of $L2$ and dimensions (height $\times$ length) of the stepped matching element ($H_{t1} \times L_{t1}$) and ($H_{t2} \times L_{t2}$) with a deviation up to 0.15 mm. The reason for the large displacement off $L3$ was the positional error of the calibrated and screwed holes. Measurements were performed in a $4 \times 4 \times 3\ m^3$ room from the UPC facilities, with a proper time gating post-processing technique, the reflections inside the room can be filtered out [25]. The measurements and simulations using CST Studio software included the reflection coefficients and realized gain patterns, which were cut at 77 GHz, and are shown in figures 13,15 and 16.

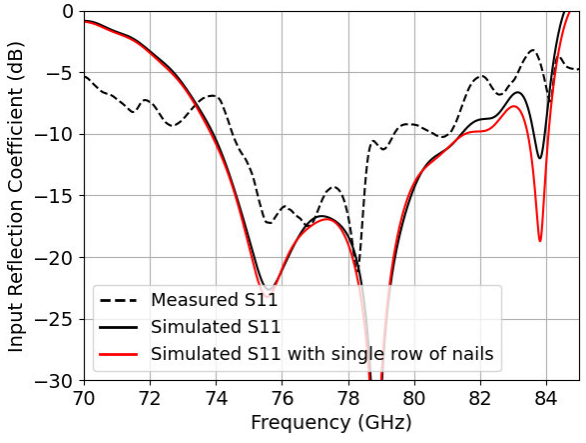

FIGURE 13. Input reflection coefficients of the antenna. In black a double row of nails for the AMC is used and in red color corresponds to the simulated antenna by just using only one row of nails to show that it can be compact in the transversal direction of the array. Discontinuous lines (- -) are the measured results while continuous lines (-) are simulated results.

There is a good correlation between the measured input reflection coefficient (74.5GHz - 81.25GHz) and the simulated one (74GHz - 81.5GHz). A portion of mismatched

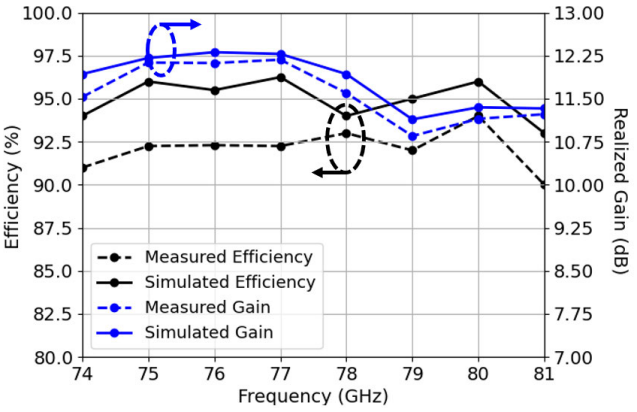

FIGURE 14. Left vertical axis corresponds to the efficiency in black and the right axis corresponds to the realized gain in blue color. Discontinuous lines (- -) are the measured results while continuous lines (-) are simulated results.

frequencies ranges from 79.25 to 80.75 GHz at only −9.1 dB. The design was performed using a double row of nails with direct contact with the upper layer, which would result in large dimensions in the transverse direction of the array. However one single row of nails is sufficient, resulting in a more compact form (0.57λ width × 1.91λ height) without altering the results (see Fig 13). The stability of the gain versus frequency for the whole band is shown in blue in the right axis of Fig. 14, with a maximum gain reduction down to 11dB at 79GHz. In the same Fig. 14 we can also see the efficiency of the antenna in black color which was measured to be greater than 90% for the whole band ranging from 74GHz to 81GHz.

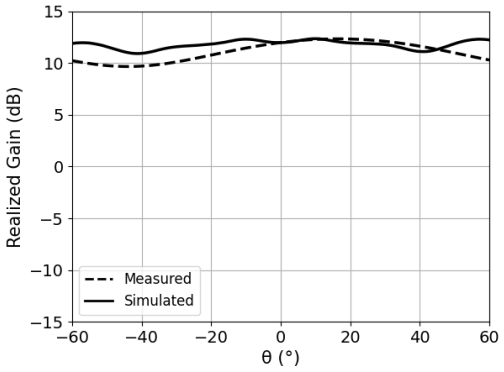

FIGURE 15. Radiation pattern cuts at E-plane, - corresponds to the simulated antenna, and - - corresponds to the actual measured prototype.

A realized gain of 12.15 dB was measured which also showed good agreement with the simulations for both planes at 77GHz. A simulated SLL of −18.5dB in H-plane was increased up to −16.5 dB at $\theta = -28$ deg in the measurements caused by the misalignment of the radiating layer l_3 with respect to the other two ones, leading to a non-perfect symmetrical field distribution among the radiating slots.

V. LIMITATIONS OF THE STUDY

In this paper we show a new method for exciting series fed slot arrays in V-GGW, although the design is easy to be scaled

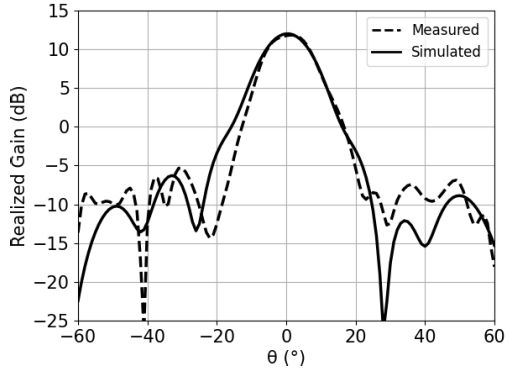

FIGURE 16. Radiation pattern cuts at H-plane, - corresponds to the simulated antenna, and - - corresponds to the actual measured prototype.

to a larger aperture antenna for 5G mmWave applications by just adding more arrays, there are some remaining studies to be done.

First, when scaling to N arrays spaced at 0.57λ (minimum achievable inter-array space with this design), a compact distribution network needs to be designed.

Second, only eight elements were used in the series-fed array. For achieving high gain levels required by future 5G mmWave applications, further studies have to be carried out by using more array elements depending on the specific 5G mmWave application and see its impact on the FBW and the tolerances in order to simplify its scalability.

VI. CONCLUSION

A single compact series-fed array antenna using a novel aperture coupling mechanism in V-GGW technology has been proposed. The measured gain of the antenna was 12.15dB by comparing it to a standard horn antenna of 23.5dB. The efficiency at 77GHz was measured to be 92.25% by assuming a directivity similar to the simulated one (12.5 dB). The antenna offers a simulated FBW of 10% which is reduced to 9% when measuring it.

The antenna shows good stability against fabrication errors of up to 0.1 mm for both input reflection coefficients and radiation pattern, which is much better than the design in RGW. It provides a minimum realized gain of 12.1dB at 77GHz for the worst case of combined errors at the simulation level and offer good tilting stability. The radiating aperture of the antenna can be increased by adding more unit arrays to increase the directivity and the frequency can be scaled depending on the specific application of future 5G mmWave wireless networks requiring massive deployments.

REFERENCES

[1] J. G. Andrews, S. Buzzi, W. Choi, S. V. Hanly, A. Lozano, A. C. K. Soong, and J. C. Zhang, "What will 5G be?" *IEEE J. Sel. Areas Commun.*, vol. 32, no. 6, pp. 1065–1082, Jun. 2014.

[2] J. Rodriguez, *Small Cells for 5G Mobile Networks*. 2014, pp. 63–104.

[3] P. Wang, Y. Li, L. Song, and B. Vucetic, "Multi-gigabit millimeter wave wireless communications for 5G: From fixed access to cellular networks," *IEEE Commun. Mag.*, vol. 53, no. 1, pp. 168–178, Jan. 2015.

[4] *FCC Advances 70-90 GHz Changes To Support Wireless 5G Backhaul*. [Online]. Available: https://www.fiercewireless.com/tech/fcc-advances-70-90-ghz-changes-to-support-wireless-5g-backhaul

[5] S. R. Zahran, L. Boccia, G. Amendola, S. Moscato, M. Oldoni, and D. Tresoldi, "Broadband D-band antenna array based on 64 stepped horns for 5G backhauling applications," in *Proc. 15th Eur. Conf. Antennas Propag. (EuCAP)*, Mar. 2021, pp. 1–5.

[6] L. Dussopt, A. Moknache, J. Säily, A. Lamminen, M. Kaunisto, J. Aurinsalo, T. Bateman, and J. Francey, "A V-band switched-beam linearly polarized transmit-array antenna for wireless backhaul applications," *IEEE Trans. Antennas Propag.*, vol. 65, no. 12, pp. 6788–6793, Dec. 2017.

[7] J. Ala-Laurinaho, J. Aurinsalo, A. Karttunen, M. Kaunisto, A. Lamminen, J. Nurmiharju, A. V. Räisänen, J. Säily, and P. Wainio, "2-D beam-steerable integrated lens antenna system for 5G *E*-band access and backhaul," *IEEE Trans. Microw. Theory Techn.*, vol. 64, no. 7, pp. 2244–2255, Jul. 2016.

[8] S. Afoakwa and Y.-B. Jung, "Wideband microstrip comb-line linear array antenna using stubbed-element technique for high sidelobe suppression," *IEEE Trans. Antennas Propag.*, vol. 65, no. 10, pp. 5190–5199, Oct. 2017.

[9] J.-H. Lee, J. M. Lee, K. C. Hwang, D.-W. Seo, D. Shin, and C. Lee, "Capacitively coupled microstrip comb-line array antennas for millimeter-wave applications," *IEEE Antennas Wireless Propag. Lett.*, vol. 19, no. 8, pp. 1336–1339, Aug. 2020.

[10] J. Hirokawa and P. S. Kildal, "Excitation of an untilted narrow-wall slot in a rectangular waveguide by using etched strips on a dielectric plate," *IEEE Trans. Antennas Propag.*, vol. 45, no. 6, pp. 1032–1037, Jun. 1997.

[11] S. C. Y. Tyagi, P. Mevada, and R. Jyoti, "High-efficiency broadband slotted waveguide array antenna," *IET Microw., Antennas Propag.*, vol. 11, no. 10, pp. 1401–1408, 2016.

[12] M. A. K. S. Lubis, C. Apriono, F. Y. Zulkifli, and E. T. Rahardjo, "Design of narrow wall slotted waveguide antenna for X-band application," in *Proc. Prog. Electromagn. Res. Symp.-Fall (PIERS-FALL)*, 2017, pp. 2625–2628.

[13] D. P. Yusuf, F. Y. Zulkifli, and E. T. Rahardjo, "Design of narrow-wall slotted waveguide antenna with V-shaped metal reflector for X-band radar application," in *Proc. Int. Symp. Antennas Propag. (ISAP)*, Oct. 2018, pp. 1–2.

[14] T. Uesaka, N. Nakamoto, T. Fukasawa, N. Yoneda, T. Yamamoto, T. Koyanagi, I. Kakimoto, and Y. Konishi, "Design of edge-slotted waveguide array antenna manufactured by injection-molding," in *Proc. IEEE Int. Symp. Phased Array Syst. Technol. (PAST)*, Oct. 2019, pp. 1–4.

[15] H. Takahashi, T. Kosugi, A. Hirata, J. Takeuchi, K. Murata, and N. Kukutsu, "Hermetic sealing technique for F-band waveguides and packages," in *Proc. 41st Eur. Microw. Conf.*, Oct. 2011, pp. 269–272.

[16] E. Rajo-Iglesias, M. Ferrando-Rocher, and A. U. Zaman, "Gap waveguide technology for millimeter-wave antenna systems," *IEEE Commun. Mag.*, vol. 56, no. 7, pp. 14–20, Jul. 2018.

[17] E. Pucci, E. Rajo-Iglesias, and P.-S. Kildal, "New microstrip gap waveguide on mushroom-type EBG for packaging of microwave components," *IEEE Microw. Wireless Compon. Lett.*, vol. 22, no. 3, pp. 129–131, Mar. 2012.

[18] S. Kildal, A. Zaman, E. Rajo, E. Alfonso, and A. Nogueira, "Design and experimental verification of ridge gap waveguide in bed of nails for parallel-plate mode suppression," *IET Microw., Antennas Propag.*, vol. 5, no. 3, pp. 262–270, 2009.

[19] E. Rajo-Iglesias and P. Kildal, "Groove gap waveguide: A rectangular waveguide between contactless metal plates enabled by parallel-plate cut-off," in *Proc. 3th Eur. Conf. Antennas Propag.*, Apr. 2010, pp. 1–4.

[20] Z. Shaterian, A. K. Horestani, and J. Rashed-Mohassel, "Design of slot array antenna in groove gap waveguide technology," *IET Microw., Antennas Propag.*, vol. 13, no. 8, pp. 1235–1239, Jul. 2019.

[21] J. I. H. Herruzo, A. Valero-Nogueira, S. M. Giner, and A. V. Jiménez, "Untilted narrow-wall slots excited by parasitic dipoles in groove gap waveguide technology," *IEEE Trans. Antennas Propag.*, vol. 63, no. 11, pp. 4759–4765, Nov. 2015.

[22] Z. Talepour, S. Esmaili, and A. Khaleghi, "Ridge gap waveguide antenna array using integrated coaxial power divider," in *Proc. Loughborough Antennas Propag. Conf. (LAPC)*, Nov. 2015, pp. 1–5.

[23] A. Haddadi, C. Bencivenni, and T. Emanuelsson, "Gap waveguide slot array antenna for automotive applications at *E*-band," in *Proc. 13th Eur. Conf. Antennas Propag. (EuCAP)*, Mar./Apr. 2019, pp. 1–4.

[24] A. Farahbakhsh, D. Zarifi, and A. U. Zaman, "60-GHz groove gap waveguide based wideband *H*-plane power dividers and transitions: For use in high-gain slot array antenna," *IEEE Trans. Microw. Theory Techn.*, vol. 65, no. 11, pp. 4111–4121, Nov. 2017.

[25] M. Dadic, R. Zentner, and Z. Lenic, "Time-gating in antenna and microwave measurements using RDFT," in *Proc. 22nd Int. Conf. Appl. Electromagn. Commun. (ICECOM)*, Sep. 2016, pp. 1–4.

IVAN ZHOU was born in Valencia, Spain, 1996. He received the degree in engineering physics and the master's degree in advanced telecommunications technologies from the Polytechnic University of Catalonia (UPC), in 2019 and 2020, respectively, where he is currently pursuing the Ph.D. degree with the Antennalab, Signal Theory and Communications Department. He was involved in millimeter wave antenna design, radome design, and ray tracing algorithms.

LLUÍS JOFRE (Life Fellow, IEEE) received the M.Sc. and Ph.D. degrees in electrical engineering (telecommunication engineering) from the Universitat Politècnica de Catalunya (UPC), Barcelona, Spain, in 1978 and 1982, respectively. He was a Visiting Professor with the Ecole Supèrieure d'Electricitè Paris, from 1981 to 1982, where he was involved in microwave antenna design and imaging techniques for medical and industrial applications. Since 1982, he has been with the Communications Department, Telecommunication Engineering School, UPC, as an Associate Professor, and then a Full Professor, since 1989. From 1986 to 1987, he was a Visiting Fulbright Scholar with the Georgia Institute of Technology, Atlanta, GA, USA, where he was involved in antenna near-field measurements and electromagnetic imaging. From 2000 to 2001, he was a Visiting Professor with the Department of Electrical and Computer Engineering, Henry Samueli School of Engineering, University of California at Irvine, CA, USA, where he was involved in reconfigurable antennas and microwave sensing of civil engineering structures. He has been the Director of the UPC-Telefonica Chair on Information Society Future Trends, since 2003. He was the Principal Investigator of the 2008–2013 Spanish Terahertz Sensing Lab Consolider Project and the Research Leader of the 2017–2020 ComSense Lab Maria de Maeztu Project. He has authored more than 200 scientific and technical articles, reports, and chapters in specialized volumes. His current research interests include antennas, electromagnetic scattering and imaging, and system miniaturization for wireless, and sensing industrial and bio-applications from microwaves to terahertz frequencies. He was the Academic Director of the Consortium for Future Urban Mobility (Carnet) and the Chairman of the EIT-Urban Mobility European Association.

JORDI ROMEU (Fellow, IEEE) was born in Barcelona, Spain, in 1962. He received the Ingeniero de Telecomunicación and Doctor Ingeniero de Telecomunicaciòn degrees from the Universitat Politècnica de Catalunya (UPC), in 1986 and 1991, respectively. In 1985, he joined the Antennalab, Signal Theory and Communications Department, UPC, where he is currently a Full Professor, and involved in antenna near-field measurements, antenna diagnostics, and antenna design. He was a Visiting Scholar with the Antenna Laboratory, University of California at Los Angeles, Los Angeles, in 1999, on an NATO Scientific Program Scholarship, and the University of California at Irvine, in 2004. He holds several patents and has published 60 refereed articles in international journals and 80 conference proceedings. He was a Grand Winner of the European IT Prize awarded by the European Commission for his contributions in the development of fractal antennas, in 1998 (More information can be found in http://www.researchgate.net/profile/Jordi−Romeu).